NASA TECHNICAL MEMORANDUM 101677

EFFECTS OF T-TABS AND LARGE DEFLECTIONS IN DCB SPECIMEN TESTS

R. A. Naik, J. H. Crews, Jr., and K. N. Shivakumar

November 1989

National Aeronautics and
Space Administration

La gley Research Center
ton, Virginia 23665

ABSTRACT

A simple strength of materials analysis was developed for a double-cantilever beam (DCB) specimen to account for geometric nonlinearity effects due to large deflections and T-tabs. A new DCB data analysis procedure was developed to include the effects of these nonlinearities. The results of the analysis were evaluated by DCB tests performed for materials having a wide range of toughnesses. The materials used in the present study were T300/5208, IM7/8551-7, and AS4/PEEK.

Based on the present analysis, for a typical deflection/crack length ratio of 0.3 (for AS4/PEEK), T-tabs and large deflections cause a 15 percent and 3 percent error, respectively, in the computed Mode I strain energy release rate. Design guidelines for DCB specimen thickness and T-tab height were also developed in order to keep errors due to these nonlinearities within 2 percent.

Based on the test results, for both hinged and tabbed specimens, the effects of large deflection on the Mode I fracture toughness (G_{Ic}) were almost negligible (less than 1 percent) in the case of T300/5208 and IM7/8551-7, however, AS4/PEEK showed a 2 to 3 percent effect. The effects of T-tabs on G_{Ic} were more significant for all the materials with T300/5208 showing a 5 percent error, IM7/8551-7 a 15 percent error, and, AS4/PEEK a 20 percent error.

Key Words: Double cantilever beam, delamination, fracture toughness, composite, large deflection, geometric nonlinearity, strain-energy release rate, loading tabs.

NOMENCLATURE

a	crack length including end correction
a_{el}	effective crack length for DCB with large deflections
a_{et}	effective crack length for DCB with T-tabs
a_{elt}	effective crack length for DCB with T-tabs and large deflections
a_{exp}, a_i	experimentally measured crack length
a_o	end correction to account for DCB crack tip rotation
b	DCB specimen width
C_i	measured initial compliance for DCB specimen
d	tab height from base to loading point
d_{exp}, δ_i	measured displacement in a DCB test
E_{11}	longitudinal composite modulus
E_{22}	transverse composite modulus
E_r	transverse modulus of resin-rich layer
G_{13}	composite shear modulus
G_I	strain-energy release rate
G_I^{et}	strain-energy release rate for DCB with T-tabs
G_I^{elt}	G_I for DCB with T-tabs and large deflections
G_{Ic}	Mode I fracture toughness
h	thickness of DCB arm
H	total tab height from loading point to center of DCB arm
$\bar{H}$	factor used in calculation of G_{Ic}
I	moment of inertia
k	foundation spring constant
M	bending moment at a section x from the crack tip

M_o	bending moment at crack tip
M_r	resisting moment due to T-tab rotation
P, P_i	applied load
t	DCB specimen thickness
t_r	thickness of resin-rich layer
w	deflection of the beam at any distance x from the crack tip
x	distance from the crack tip
δ_A	deflection of DCB arm
Δ_l	crack length shortening due to large deflections
Δ_t	crack length shortening due to T-tab rotation
θ	angle of rotation at DCB loading point

INTRODUCTION

The double cantilever beam (DCB) specimen is a popular specimen for determination of composite Mode-I interlaminar fracture toughness (G_{Ic}). DCB specimens usually consist of several unidirectional plies layed-up with a thin insert at the midplane (Fig. 1) to serve as a starter crack. Load is applied either through metal hinges [1 - 8] or metal T-tabs [9 - 16] bonded to the end of the specimen. The crack length is measured along the specimen edges. The measured crack length, applied load, and load-point deflection are then used to compute G_{Ic} by a data analysis method which is usually based on linear beam theory [1,2,5-8,12-18].

In general, the DCB specimen is designed to limit deflections to the geometrically linear range [1,2]. However, with the advent of tough resin composites, there is an increased possibility of encountering large deflections for DCB specimen thicknesses that have been conventionally used.

Large deflections cause an effective shortening of the crack length (Fig. 2(a)) which leads to errors in the computed G_{Ic} values if DCB data are analyzed using linear beam theory assumptions. In such instances, for a chosen DCB specimen design, an estimate of the effect of large deflections on the computed G_{Ic} values can be made by the analyses of references 3 and 4. Alternatively, the design criteria suggested in references 1 and 2 can be used to limit DCB deflections to the geometrically linear range.

As mentioned earlier, the DCB specimen is loaded either through bonded hinges or T-tabs. The use of T-tabs shifts the line of action of the load due to the rotation of the DCB arms and leads to an effective crack-length shortening (Fig. 2(b)). The use of hinged tabs drastically reduces this effect. The effective crack-length shortening in the case of T-tabs increases with load [9-11] and leads to a geometrically nonlinear problem. The analyses in references 9 and 11 account for the geometric nonlinearities resulting from both T-tabs and large deflections. Wang et. al [9] and Williams [11] state that the effects of loading tabs significantly contribute to the strain-energy release rate in a DCB specimen.

Hinged DCB specimens are, therefore, preferable to T-tabbed specimens. T-tabs may be required for some tough materials, however, because of the larger critical loads. Although the effect of end rotation on computed G_{Ic} values could be accurately accounted for by the analyses in references 9 and 11, these analyses are quite complicated and tedious to use. Conversely, T-tabs could be designed to minimize the effects of end rotation. However, there are no design guidelines available for DCB specimen tabs.

The purpose of this paper is first to present a simple strength of materials analysis to account for geometric nonlinearities resulting from T-tabs and large deflections. Next, DCB design guidelines are presented to

minimize the effects of these geometric nonlinearities. Then, a data analysis procedure is developed to compute G_{Ic}. Finally, DCB test results are presented to quantify these effects for commonly used composites over a wide range of toughnesses.

MATHEMATICAL ANALYSIS OF DCB SPECIMEN WITH T-TABS

The analysis of a DCB specimen with T-tabs is presented in the following sections. The DCB arm is first idealized as a beam on an elastic foundation. Equations for the load-deflection behavior are then derived for the case of small deflections followed by derivations for the case of large deflections. Next, expressions for the strain-energy release rate are derived for a DCB with T-tabs. Finally, design guidelines are developed to ensure that DCB deflections are in the geometrically linear range.

The DCB specimen arm can be represented as a beam on an elastic foundation [18]. The deflection of such a beam with an elastic foundation can be approximated by the deflection of a cantilever beam with an additional end correction length of a_o (see Appendix). Thus, for the DCB specimen shown in figure 3, each arm of the DCB can be idealized as a cantilever beam of length a given by

$$a = a_{exp} + a_o \tag{1}$$

where a_{exp} is the crack length measured during testing (see Figs. 1, 3 and 4) and a_o is given by (see Appendix):

$$a_o = h \sqrt[4]{(E_{11}/6\ E_{22})} \qquad (2)$$

where h is the thickness of each arm; E_{11} and E_{22} are the longitudinal and transverse moduli, respectively.

Small Deflection Analysis

Consider a DCB specimen that has bonded T-tabs of height d (Fig. 3). The application of load P causes an end rotation θ which results in a resisting moment M_r (Fig. 3) given by

$$M_r = P\ H \sin(\theta) \qquad (3)$$

where,

$$H = d + (h/2) \qquad (4)$$

Note that the tabs are assumed to be rigid in the present analysis. Thus, a DCB specimen with load P applied through end tabs and a measured crack length of a_{exp} can be analyzed as a cantilever beam of length a (Eq.(1)) with load P and a resisting moment M_r (see Fig. 3). Note that M_r is a function of θ which in turn is a function of P leading to a geometrically nonlinear problem.

The cantilever beam in figure 3 can be analyzed by first writing the moment at any point x along the beam and then using the moment-curvature relationship for a beam. The moment at any point x along the beam is,

$$M(x) = P\ (a - x) - P\ H \sin(\theta) \qquad (5)$$

The moment-curvature relationship for the beam is given by [19],

$$\frac{d^2w}{dx^2} = \frac{M}{E_{11} I} \tag{6}$$

where I is the moment of inertia of the beam cross-section and w is the beam deflection at any point along the beam. Note that the flexural rigidity of the tabs is neglected in the above equation. Integrating and applying the appropriate boundary conditions yields expressions for the slope and deflection at the point A (see Fig. 3). The slope is given as

$$\tan(\theta) = \left(\frac{P a^2}{2 E_{11} I}\right)\left(1 - 2 \frac{H}{a}\sin(\theta)\right) \tag{7}$$

and the deflection δ_A at point A is given by,

$$\delta_A = \left(\frac{P a^3}{3 E_{11} I}\right)\left(1 - 1.5 \frac{H}{a}\sin(\theta)\right) \tag{8}$$

Note that equations (7) and (8) agree with the slope and deflection of a linear beam (with load P) when H is set equal to zero.

As shown in figure 2, the loading tabs cause an effective shortening (Δ_t) of the beam length. This shortening can be easily determined, by inspection of figures 3 and 4, as $(H \sin(\theta))$. The effective length of a beam with T-tabs can, thus, be approximated by a_{et} where,

$$a_{et} = a \left(1 - \frac{H}{a}\sin(\theta)\right) \tag{9}$$

This effective length a_{et} will be used later in the derivation of Mode I strain-energy release rate for a DCB with T-tabs. Note that a_{et} from the above equation can be used in the deflection equation of a linear cantilever beam to approximate the deflection of a linear beam with tabs; however, that would give the deflection at point A′ (see Fig. 3) on the beam and not at point A. Note that, A′ is not a fixed point on the beam and does not provide a good reference for beam deflection and thus the point A is used as a reference for beam deflection. The deflection at point A given by equation (8) can also be related to the measured (load-point) displacement in a tabbed DCB test. This measured deflection d_{exp} (see Fig. 4) can be expressed as,

$$d_{exp} = 2\,(\delta_A + H\,(\cos(\theta) - 1)) \qquad (10)$$

The load-deflection behavior of a DCB with tabs can now be examined by using equations (7), (8) and (10).

Figure 5 shows a plot of DCB load verses load-point deflection. Both the quantities are presented in a nondimensional form. The dash-dotted curve represents the load-deflection behavior of a linear DCB with tabs for a H/a ratio of 0.3 which represents a 25.4 mm tab and a crack length of 85 mm. Note that, the crack lengths used in a DCB test are usually between 50 mm and 120 mm. For deflection/length ratios of less than 0.05, the DCB with tabs closely follows the simple linear DCB with hinges (dotted line). However, for larger d_{exp}/a ratios, the DCB with tabs departs considerably from linear beam behavior. For a DCB specimen (3 mm thick) made from AS4/PEEK, initial crack extension occurs at a d_{exp}/a ratio of about 0.3 under static loading [15].

At this ratio there is a difference of 18 percent between a DCB with tabs and a DCB with hinges.

Large Deflections Analysis

The effects of large deflections on DCB response has been studied in references 3, 4, 9, and 11. DCB specimens with hinges were considered in references 3 and 4, while tabbed DCB's were analyzed in references 9 and 11. The analyses in references 9 and 11, however, are very complicated and do not separate the effects of T-tabs and large deflections. The present study uses a simple strength of materials approach, similar to that in reference 4, to analyze a DCB with tabs undergoing large deflections.

As discussed earlier, large deflections cause an effective shortening of the crack length (see Fig. 2). This shortening can be derived by considering the x-axis strain at the midplane of the beam. The strain ϵ_x at the midplane is given by [20]

$$\epsilon_x = \frac{\partial u}{\partial x} + (1/2)\left(\frac{\partial w}{\partial x}\right)^2 \qquad (11)$$

where u and w are displacements in the x and y directions, respectively. The midplane strain ϵ_x is assumed to be zero [4]. Thus, the variation of u with respect to x is given by

$$\partial u/\partial x = -1/2(\partial w/\partial x)^2 \qquad (12)$$

The term $(\partial w/\partial x)$ can be obtained from equations (5) and (6) for a DCB with tabs and is given by

$$\frac{\partial w}{\partial x} = \left(\frac{P}{2 E_{11} I}\right)\left(a^2 - (a - x)^2 - 2 x H \sin(\theta)\right) \qquad (13)$$

Integrating equation (12) along the beam length after substituting for $\partial w/\partial x$ from equation (13) gives the total shortening Δ_1 of the beam in the x-direction as

$$\Delta_1 = \int_0^a \left(\frac{\partial u}{\partial x}\right) dx \qquad (14a)$$

i.e.

$$\frac{\Delta_1}{a} = (1/3)\left(\frac{P a^2}{E_{11} I}\right)^2\left((1/5) - (5/8)(H/a)\sin(\theta) + (1/2)(H/a)^2\sin^2(\theta)\right) \qquad (14b)$$

The effective crack length (a_{el}) for a beam with large deflections is thus

$$a_{el} = a\,(1 - (\Delta_1 / a)) \qquad (15)$$

Using equations (9) and (15) it is clear that the effective crack length for a DCB arm with tabs undergoing large deflections can be written as

$$a_{elt} = a\,\left(1 - \frac{H}{a}\sin(\theta) - (\Delta_1 / a)\right) \qquad (16)$$

This effective crack length for a DCB arm with T-tabs undergoing large deflections will be used later in the derivation of Mode I strain-energy release rate. Note that, if the effective crack length a_{elt} is used in the deflection equation of a linear beam in order to account for the effects of

tabs and large deflections, then that would give the deflection at point A' and not at point A.

The deflection, at point A, of a DCB arm with tabs that is undergoing large deflections can be written, using equations (8) and (15) as

$$\delta_A = \left(\frac{P\,a^3}{3\,E_{11}\,I}\right)\left(1 - 1.5\,\frac{H}{a}\sin(\theta)\right)\left(1 - (\Delta_1/a)\right)^3 \qquad (17)$$

The nonlinear load-deflection response of a DCB with tabs can be plotted using equations (7), (10), (14), and (17) and is shown in Fig. 5 (solid curve). At a typical d_{exp}/a ratio of 0.3 [15] and a H/a ratio of 0.3, the nonlinear tabbed DCB (solid curve) is 6 percent above the linear tabbed DCB (dash-dotted curve) and 25 percent above the linear hinged DCB (dotted curve). The load-deflection curve for the DCB with tabs and large deflections (solid curve) obtained by the present analysis agrees well with that obtained by the more accurate analysis of reference 9 (short dashed curve) for d_{exp}/a ratios of less than 0.4. However, for d_{exp}/a ratios of 0.4 and greater there is more than 6 percent difference between the present analysis and that of reference 9. The effect of large deflections in the absence of T-tabs can be examined by using equations (14) and (17) and substituting $H = 0$. This leads to the long dashed curve in figure 5 for a hinged nonlinear DCB. For a typical d_{exp}/a ratio of 0.3, the effect of large deflections in a hinged DCB is only 3 percent.

Strain-Energy Release Rate Analysis

Based on the deflection equation for a linear DCB with tabs (equation (8)) and its similarity to the linear cantilever beam equation, it is possible to derive a simple equation for the strain-energy release rate. As discussed earlier, the geometric nonlinearities associated with large deflections and T-tabs lead to an effective shortening of the beam. Equations (9), (14), and (15) give a good estimate of this shortening as a function of the applied load.

The strain-energy release rate G_I for the DCB is given by [4]

$$G_I = \frac{M_o^2}{b\, E_{11}\, I} \tag{18}$$

where b is the width of the specimen and M_o is the bending moment at the crack tip. For a linear hinged DCB, M_o is given simply by $(P\ a)$. Equation (18) is valid for a linear hinged DCB, however, it has been shown in references 4 and 11 that it can be used for a DCB with geometric nonlinearities if the moment is calculated by taking into account the shortening of the DCB arm. Thus if M is given by $(P\ a_{et})$ for a linear tabbed DCB (see equation (9)) and by $(P\ a_{elt})$ for a tabbed DCB with large deflections (see equation (16)) then equation (18) can also be used for these cases. The strain-energy release rate for a linear DCB with tabs can, therefore, be written as

$$G_I^{et} = \left(\frac{P^2 a^2}{b E_{11} I}\right)\left(1 - \frac{H}{a}\sin(\theta)\right)^2 \qquad (19)$$

Note that a in the above equation is the sum of the measured crack length a_{exp} and the end correction a_o (see equation (1)). The angle θ is a function of the applied load (see equation (7)).

For a DCB with tabs undergoing large deflections, the expression for G_1 is given by,

$$G_I^{elt} = \left(\frac{P^2 a^2}{b E_{11} I}\right)\left(1 - \frac{H}{a}\sin(\theta) - (\Delta_1 / a)\right)^2 \qquad (20)$$

where Δ_1 / a is the shortening in the crack length due to large deflections and is given by equation (14). The effects of both large deflections and T-tabs on the strain-energy release rate in a DCB can now be studied for a range of d_{exp}/a ratios by using equations (7), (8), (10), (14), (17), (19), and (20).

Figure 6 shows the normalized strain-energy release rate $(G_I b a^2/E_{11} I)$ as a function of the normalized DCB load-point deflection (d_{exp}/a) for a H/a ratio of 0.3. For d_{exp}/a ratios of less than 0.3, the short dashed curve for a linear DCB with tabs differs by less than 4 percent from the results, for a linear DCB with tabs, from reference 10 (dash-dotted curve). At d_{exp}/a ratios greater than 0.3, the agreement is not very good; but for such high ratios there will be large deflections in the DCB specimen; and, one should use the results for the large deflection case. The solid curve in figure 6 corresponds to a DCB with tabs and large deflections (equation (20)) and compares very well with the result from reference 9. For a typical d_{exp}/a ratio of 0.3 [15], the present solution differs by only 2 percent from the

more accurate solution of reference 9. Also, for d_{exp}/a ratios greater than 0.3 there is a very good correlation between the present solution and that of reference 9.

Figure 7 shows the effect of tab height for a range of H/a ratios (based on equation (20)). The solid curve corresponds to a nonlinear hinged DCB and was obtained from equation (20) by substituting H/a equal to zero. For a typical d_{exp}/a ratio of 0.3, the results for the nonlinear hinged DCB differ by only 3 percent from those for the linear hinged DCB (dotted curve). The results for the linear hinged DCB were obtained by substituting H/a equal to zero in equation (19). The difference between the linear hinged DCB and the nonlinear tabbed DCB increases with increasing H/a ratios.

The percentage variation from the linear beam theory assumptions for DCB specimens, that have T-tab and/or large deflection effects, are summarized in figure 8 for a range of d_{exp}/a ratios and a H/a ratio of 0.3. For a nonlinear hinged DCB, the percentage error in using linear beam theory analysis is less than 5 percent for d_{exp}/a ratios of less than 0.4. However, for a DCB with tabs ($H/a = 0.3$) undergoing large deflections, there could be errors as high as 18 percent (for a d_{exp}/a of 0.3) if one uses linear beam theory assumptions. For a linear DCB with tabs ($H/a = 0.3$) there would be a 15 percent error, for a d_{exp}/a of 0.3, if one did not account for the effects of the tabs.

Guidelines for Minimizing Geometric Nonlinearity Effects

The G_I expressions in the previous section can also be used to derive design criteria for DCB specimens with T-tabs and large deflections to ensure that DCB deflections are in the geometrically linear range.

DCB Specimens with Large Deflections

Consider a hinged DCB specimen which is undergoing large deflections. The expression for G_I in this case can be derived from equation (20) by substituting H equal to zero and the corresponding expression for Δ_1 from equation (14)

$$G_I = \left(\frac{P^2 a^2}{b E_{11} I}\right)\left(1 - (1/15)\left(\frac{P a^2}{E_{11} I}\right)^2\right)^2 \qquad (21)$$

Notice, that the first term in the above equation corresponds to the G_I for a linear DCB and the second term corresponds to a correction attributable to large deflections. If one desires to limit large deflection effects to, say, less than 2 percent, then the following inequality should hold true:

$$\left(1 - (1/15)\left(\frac{P a^2}{E_{11} I}\right)^2\right)^2 \geq 0.98 \qquad (22)$$

Using the above inequality and equation (21) and substituting for I appropriately, an inequality for laminate thickness t can be written as

$$t \geq 8.65 \sqrt[3]{(G_{Ic} a^2 / E_{11})} \qquad (23)$$

where G_{Ic} is the Mode I fracture toughness for the material being tested and a is the crack length of the DCB specimen. The laminate thickness used for a DCB specimen should satisfy the condition above in order to ensure less than 2 percent effects due to large deflections. The above inequality could also be

used to find the crack length a for which errors due large deflection will be less than 2 percent. If the G_{Ic} value for crack extension from the insert is of interest then, in order to keep large deflection effects below 2 percent, the insert length should be less than $(0.04 \sqrt{(t^3 E_{11}/G_{Ic})}$ for a given laminate thickness t.

DCB Specimens with T-tabs

The expression for G_I, in the case of a DCB specimen with tabs, was derived earlier (see equation (19)). In equation (19), the first term corresponds to the G_I for a linear DCB and the second term corresponds to a correction attributable to the effects of T-tabs. If one desires to limit T-tab effects to less than 2 percent, then the following inequality should hold true:

$$(1 - \frac{H}{a}\sin(\theta))^2 \geq 0.98 \qquad (24)$$

Using the above inequality and equations (7) and (19) and substituting for I appropriately, an inequality for total tab height H can be written as

$$H \leq 0.01 \sqrt{(0.0434 E_{11} t^3/G_{Ic}) + a^2)} \qquad (25)$$

Note that H is the total tab height and is given by equation (4). The tab height used in a DCB specimen with tabs should satisfy the condition above in order to ensure less than 2 percent effects due to the tabs. For a hinged specimen H corresponds to the height of the hinge axis of rotation above the

centerline of the DCB arm. For DCB specimens that are made thicker in order to minimize large deflection effects, the distance H even for hinge tabs could be significant and equation (25) should be used to check for this tab-like effect.

DCB TESTING AND DATA ANALYSIS

The results of the analysis in earlier sections suggests that the effects of geometric nonlinearity associated with T-tabs, on the computed G_I values, can be as high as 18 percent, while the effects of large deflection will usually be less than 5 percent. In order to illustrate these results, specimens made from unidirectional composites having a wide range of Mode I fracture toughness values were tested both as hinged DCB's and as tabbed DCB's. The DCB data was analyzed using three different procedures. First, a data analysis procedure based on the present analysis was used to account for large deflection and T-tab effects. Next, the well known Berry procedure [17] based on linear beam theory was used. Finally, the area method was used to provide an accurate reference for comparing average G_{Ic} values.

Materials and Specimens

Specimens were about 3 mm thick and were cut from unidirectional, 24 ply, panels with a Kapton film (0.0127 mm thick) crack starter at the midplane. Three different panels were made from T300/5208, IM7/8551-7 [21], and AS4/PEEK prepreg according to the manufacturer's instructions. After curing, the panels were cut into 152 mm by 25 mm DCB specimens. Only two specimens of

each material were tested since the focus of the present tests was to illustrate the analysis and compare different data analysis procedures. For each material, one of the specimens was bonded with aluminum alloy hinges and another was bonded with aluminum T-tabs that were 25 mm in height (d = 25 mm, see Fig. 3). Edges of the specimens were painted with white water-based typewriter correction fluid and marked at increments of 2.5 mm for visual crack measurements.

Test Procedure

Static tests were performed under displacement control in a screw-driven machine at a constant cross-head rate of 0.0085 mm/s. Load-deflection data was collected through a digital data acquisition system and was also plotted on a x-y plotter. Travelling microscopes were used to monitor crack length along both edges of the specimen. Load and deflection were noted for the initial crack extension from the insert and then at every 2.5 mm of crack extension indicated by the marks on the specimen edges. After the crack had extended about 12.7 mm the specimen was unloaded. The specimen was reloaded and the crack was extended another 12.7 mm while the load, deflection, and crack length were monitored. A third loading-unloading cycle was conducted in a similar manner for another 12.7 mm of crack extension. Typical load-deflection plots are shown schematically in figure 9. The geometric nonlinearities associated with T-tabs and large deflections cause an upwardly concave curve with a monotonically decreasing compliance. The initial compliance, denoted by C_i, will be used later in the data analysis procedure.

Data Analysis Procedures

As mentioned earlier, data analysis was performed using three different procedures. This section describes the present analysis to account for the effects of large deflections and T-tabs, Berry's [17] procedure and the area method.

Present Data Analysis Procedure

The present procedure uses the initial compliance C_i (Fig. 9), the load, deflection, and crack length data, and the G_I expression given by equation (20) to determine G_{Ic}. There are, however, two unknowns in equation (20) that need to be determined before that equation can be used to determine G_{Ic}. These two unknowns are the flexural stiffness $E_{11}I$ and the angle θ at the end of the DCB arms.

The quantity $E_{11}I$ is directly evaluated by compliance calibration in the present data analysis procedure. However, as indicated in figure 9, the compliance of a DCB with geometric nonlinearities changes with load. Based on the analysis, the load-deflection plots in figure (5) also indicate a compliance that changes with load but for very small deflections ($\delta/a < 0.05$), the curves for the geometrically nonlinear cases coincide with the linear beam curve. Thus the effects of large deflections and T-tabs are minimal for the initial part of the load-deflection curve and the initial compliance C_i can be approximated by linear beam theory assumptions as

$$C_i = \left(\frac{2}{3\ E_{11} I}\right) a^3 \qquad (26)$$

The quantity in brackets can be determined from a least-squares fit on a log-log plot of C_i versus a. This method was used to determine $E_{11}I$ in the present data analysis procedure.

The above procedure eliminates the errors involved in using the values of E_{11} and I in the computation of G_{Ic}. The quantity E_{11} in equation (20) is actually an effective modulus which, in general, is not the same as the inplane modulus [1,2,13]. Furthermore, the E_{11} in a composite could vary along the laminate thickness due to inhomogeneity caused by the manufacturing process [22]. Also, the moment of inertia I (= $(1/12)\ b\ h^3$) contains h^3 which could lead to large errors in the computed I due to even small errors in measuring laminate thickness.

The angle θ at the end of the DCB arms was determined by using the load-deflection relation derived earlier (equation (17)) together with the result from equation (10). The measured deflection can thus be written as

$$d_{exp} = \left(\frac{2\ P\ a^3}{3\ E_{11}\ I}\right)\left[1 - 1.5\ \frac{H}{a}\sin(\theta)\right] + 2\ H\ (\cos(\theta) - 1) \qquad (27)$$

A shear correction term [8] given by $(2.4\ P\ a/(b\ h\ G_{13}))$ could be added to the above equation where G_{13} is the shear modulus and $E_{11}I$ is determined as discussed earlier. The measured load P, deflection d_{exp} and crack length a (given by equation (1)) are substituted into equation (27) to determine the angle θ iteratively by a numerical scheme. The secant method was used in the present study.

Once the quantities $E_{11}I$ and θ are known, the G_{Ic} for the material can be computed by

$$G_{Ic} = \left(\frac{P^2 a^2}{b E_{11} I}\right)\left[1 - \frac{H}{a}\sin(\theta) - (\Delta_1/a)\right]^2 \qquad (28)$$

where (Δ_1/a) is given by equation (14). A shear correction term [8] given by $(1.2\ P^2/(b^2\ h\ G_{13}))$ could be added to the above equation to account for shear deformation. Note that the term $((H/a)\sin(\theta))$ corresponds to a correction due to T-tabs and should be used only for a DCB with tabs. Also, the term (Δ_1/a) corresponds to a correction due to large deflections.

Alternatively, the G_{Ic} could also be calculated by first determining $E_{11}I$, as described earlier, and then using figure 7 along with the measured d_{exp}/a ratio at crack extension and the H/a ratio to find the corresponding value for $(G_I b\ a^2/E_{11}I)$. Knowing b, a, and $E_{11}I$, one can find G_I and then calculate G_{Ic} by adding the shear correction of equation (28) to G_I.

Berry's Method

The mode I fracture toughness can be determined by Berry's method [17] which uses the load, load-point deflection, and crack length data at the time of crack extension in the following equation [13]:

$$G_{Ic} = \frac{n\ \bar{H}}{2\ b} \qquad (29)$$

where,

$$\bar{H} = (1/N)\sum_{i=1}^{N}\left(\frac{P_i \delta_i}{a_i}\right) \qquad (30)$$

where P_i, δ_i, and a_i are the measured load, deflection, and crack length, respectively, and N is the total number of data points while n is the slope of the least-squares fit to the compliance-crack length data plotted on a log-log scale. This method has the advantage of not requiring $E_{11}I$ as the input parameter. Also, since the load, deflection, and crack length are all used in the computation, it might account, at least in part, for the effects of geometric nonlinearity. However, Berry's method is based on linear beam theory and does not explicitly account for the effects of T-tabs and large deflections.

The Area Method

The load-deflection plots shown in figure 9 can be used directly to compute G_{Ic} by accurately measuring the area enclosed by the loading-unloading curve and dividing it by the incremental area created during crack extension. This method implicitly accounts for any geometric nonlinearities since it uses the actual load-displacement curves. However, it can only give average G_{Ic} values and cannot be used to compute the G_{Ic} at the onset of crack growth from the insert.

RESULTS AND DISCUSSION

The DCB data for the three different materials was used to compute G_{Ic} for both the hinged and the tabbed specimens. The present data analysis method was used by including all the geometric nonlinearity terms and then also used by neglecting the effects of large deflections and T-tabs. Table 1 shows a comparison of the G_{Ic} values computed using the present method,

Berry's method and the area method. The values shown in the second through fifth columns are for the onset of delamination from the insert while the values shown in the last two columns are average values for the first 12.7 mm of crack extension. The values calculated using Berry's method (BM) should be compared with those from the present method obtained by neglecting the effects due to tabs and large deflections (LB). In general, there is good agreement between these two methods and the slight differences can be attributed to the differences in the two methods of data analysis. The average G_{Ic} values shown in the last two columns are subject to the effects of fiber-bridging and are therefore higher than those computed for the onset of delamination. However, a comparison of these two columns helps validate the results of the present analysis technique.

Table 1 also shows G_{Ic} values computed using the present data analysis method after separately accounting for large deflection (LDT) and T-tab (TB) effects. For both hinged and tabbed specimens the effects of large deflection were less than 0.8 percent in the case of T300/5208 and IM7/8551-7, and about 3 percent for AS4/PEEK. The effects of T-tabs were more significant for all the materials with T300/5208 showing a 5 percent effect, IM7/8551-7 a 15 percent effect, and, AS4/PEEK a 20 percent effect.

The effects due to large deflections and T-tabs could have been avoided for the three materials if the DCB thickness and T-tab height were selected according to the guidelines given by equations (23) and (25). For T300/5208, the two equations yield (using $G_{Ic} = 87.5$ J/m^2, $E_{11} = 181.3$ GPa, $a = 64$ mm) $t \geq 1.08$ mm and $H \leq 16$ mm. In the present study a laminate thickness of 3 mm and $H = 25.75$ mm were used, thus, leading to negligible large deflection effects and small T-tab effects. For AS4/PEEK, the guidelines of equations (23) and (25) yield (using $G_{Ic} = 1622$ J/m^2, $E_{11} = 136.5$ GPa, $a = 64$ mm) $t \geq$

3.14 mm and $H \leq 4$ mm. The laminate thickness used in this case was 3.23 mm, thus, explaining large deflection errors of about 2 percent (see Table 1). The tab height H used was 25.8 mm which is much higher than the recommended 4 mm leading to the 20 percent errors due to T-tab effects.

CONCLUDING REMARKS

A simple strength of materials analysis was developed for a DCB specimen to account for geometric nonlinearity effects due to large deflections and tabs. A new DCB data analysis procedure was developed to include the effects of these nonlinearities. The results of the analysis were validated by DCB tests performed for materials having a wide range of toughnesses. The materials used in the present study were T300/5208, IM7/8551-7, and AS4/PEEK.

The results of the present simple analysis compared very well with previously developed, more complicated analyses. Based on the analysis, for a typical deflection/crack length ratio of 0.3 (for AS4/PEEK) and a H/a ratio of 0.3, there could be a 19 percent effect due to T-tabs and a 6 percent effect due to large deflections on the DCB load-deflection response. The computed strain-energy release rates can be in error by 15 percent due to tabs and by 3 percent due to large deflections for the same deflection/crack length ratio of 0.3. In order to keep errors due to these nonlinearities within 2 percent the DCB specimen thickness should be greater than $8.65 \sqrt[3]{(G_{Ic}\ a^2/E_{11})}$ and the total tab height should be less than $0.01 \sqrt{(0.0434\ E_{11}\ t^3/G_{Ic}) + a^2}$.

Based on the test results for both hinged and tabbed specimens, the effects of large deflection were almost negligible (less than 1 percent) in the case of T300/5208 and IM7/8551-7, however, AS4/PEEK showed a 2 to 3

percent effect. The effects of T-tabs were more significant for all the materials with T300/5208 showing a 5 percent effect, IM7/8551-7 a 15 percent effect, and, AS4/PEEK a 20 percent effect. The average G_{Ic} values computed using the present analysis compared well with those calculated using the area integration method.

APPENDIX

The end deflection of an orthotropic beam on an elastic foundation can be written in a form similar to that given for an isotropic beam in reference [18] and is given as

$$\delta = \left(\frac{P\,a^3}{3\,E_{11}\,I}\right)\left(1 + 3/(\lambda a) + 3/(\lambda a)^2 + 1.5/(\lambda a)^3\right) \qquad \text{(A1)}$$

where,

$$\lambda = \sqrt[4]{((0.25\,k)/(E_{11}\,I))} \qquad \text{(A2)}$$

and k is the spring constant of the elastic foundation. In the case of a DCB specimen the elastic foundation consists of a thin resin rich layer (of thickness t_r) that forms in between two plies and an orthotropic laminate layer (of thickness h) [23]. The combined stiffness of the two layers represents the foundation spring constant k. By assuming a constant strain in the resin rich layer and a linearly varying strain distribution in the laminate layer [23] the tranverse stiffnesses are given by $(E_r\,b/t_r)$ and $(2\,E_{22}\,b/h)$, respectively (where b is DCB width). Since the resin rich layer and the laminate layer are in series, the foundation spring constant is given by

$$k = \frac{2\ E_r\ E_{22}\ b}{2\ E_{22}\ t_r + E_r\ h} \tag{A3}$$

For a very thin resin rich layer equation (A3) can be simplified as

$$k = 2\ E_{22}\ b/h \tag{A4}$$

and from equation (A2)

$$1/\lambda = h\ \sqrt[4]{(E_{11}/6\ E_{22})} \tag{A5}$$

Now, equation (A1) can be approximated by replacing 1.5 in the last term with 1.0 as

$$\delta = \left(\frac{P}{3\ E_{11}\ I}\right)(a + a_o)^3 \tag{A6}$$

where

$$a_o = 1/\lambda \tag{A7}$$

Note that equation (A6) represents the load-point deflection of a cantilever beam of length $(a + a_o)$ and thus a beam on elastic foundation could be approximated by a cantilever beam with an "end correction" a_o which is given from equations (A5) and (A7) by

$$a_o = h\ \sqrt[4]{(E_{11}/6\ E_{22})} \tag{A8}$$

Since the present analysis is primarily for static DCB tests, only the extensional stiffness of the foundation was considered while it's rotational stiffness was neglected. It has been shown in reference 24 that for static cases the rotational stiffness can be neglected but it should be included in analyzing dynamic cases.

REFERENCES

1. Ashizawa, M.: "Improving Damage Tolerance of Laminated Composites through the use of new Tough Resins," Douglas Paper 7250, 1983, McDonnell Douglas Corporation, Long Beach, California 90846.
2. "Standard Tests for Toughened Resin Composites," Revised Edition, NASA Reference Publication 1092, July 1983, National Aeronautics and Space Administration.
3. Devitt, D. F., Schapery, R. A., and Bradley, W. L.: "A Method for Determining the Mode I Delamination Fracture Toughness of Elastic and Viscoelastic Composite Materials," Journal of Composite Materials, Vol. 14, October 1980, pp.270-285.
4. Whitcomb, J. D.: "A Simple Calculation of Strain-Energy Release Rate for a Nonlinear Double Cantilever Beam," Journal of Composites Technology & Research, September 1984, pp.64-66.
5. Martin, R. H.: "Effect of Initial Delamination on G_{Ic} and G_{Ith} values from Glass/Epoxy Double Cantilever Beam Tests," Proceedings of the American Society for Composites, Seattle, Washington, September 1988, pp.688-700.

6. Johnson, W. S. and Mangalgiri, P. D.: "Investigation of Fiber Bridging in Double Cantilever Beam Specimens," Journal of Composites Technology & Research, Vol. 9, 1987, pp.10-13.

7. Chai, H.: "The Characterization of Mode I Delamination Failure in Non-Woven, Multidirectional Laminates," Composites, Vol. 15, October 1984, No. 4, pp.277-290.

8. Aliyu, A. A. and Daniel, I. M.: "Effects of Strain Rate on Delamination Fracture Toughness of Graphite/Epoxy," Delamination and Debonding of Materials, ASTM STP 876, W. S. Johnson, Ed., American Society for Testing and Materials, Philadelphia, 1985, pp.336-348.

9. Wang, S. S., Suemasu, H., and Zahlan, N. M.: "Interlaminar Fracture of Random Short-Fiber SMC Composite," Journal of Composite Materials, Vol. 18, November 1984, pp.574-594.

10. Wang, S. S. and Miyase, A.: "Interlaminar Fatigue Crack Growth in Random Short-Fiber SMC Composite," Journal of Composite Materials, Vol. 20, September 1986, pp.439-456.

11. Williams, J. G.: "Large Displacement and End Block Effects in the 'DCB' Interlaminar Test in Modes I and II," Journal of Composite Materials, Vol. 21, April 1987, pp.330-347.

12. Hwang, W. and Han, K. S.: "Interlaminar Fracture Behavior and Fiber Bridging of Glass-Epoxy Composite under Mode I Static and Cyclic Loadings," Journal of Composite Materials, Vol. 23, April 1989, pp.396-430.

13. Whitney, J. M., Browning, C. E. and Hoogsteden, W.: "A Double Cantilever Beam Test for Characterizing Mode I Delamination of Composite Materials," Journal of Reinforced Plastics and Composites, Vol. 1, October 1982, pp.297-313.

14. Wilkins, D. J., Eisenmann, J. R., Camin, R. A., Margolis, W. S. and Benson, R. A.: "Characterizing Delamination Growth in Graphite-Epoxy," Damage in Composite Materials, ASTM STP 775, K. L. Reifsnider, Ed., American Society for Testing and Materials, 1982, pp.168-183.

15. Russell, A. J. and Street, K. N.: "The Effect of Matrix Toughness on Delamination: Static and Fatigue Fracture," Toughened Composites, ASTM STP 937, N. J. Johnston, Ed., American Society For Testing and Materials, Philadelphia, 1987, pp.275-294.

16. Guedra, D., Lang, D., Rouchon, J., Marias, C. and Sigety, P.: "Fracture Toughness in Mode I: A Comparison Exercise of Various Test Methods," Proceedings of the sixth International Conference on Composite Materials, ICCM & ECCM, London, UK, July 1987, Vol. 3, pp.346-357.

17. Berry, J. P.: "Determination of Fracture Energies by the Cleavage Technique," Journal of Applied Physics, Vol. 34, No. 1, January 1963, pp.62-68.

18. Kanninen, M. F.: "An Augmented Double Cantilever Beam Model for Studying Crack Propagation and Arrest," International Journal of Fracture, Vol. 9, No. 1, March 1973, pp.83-91.

19. Timoshenko, S. and Young, D. H.: "Elements of Strength of Materials," Fifth Edition, Published by Van Nostrand Reinhold Company, N. Y., 1968.

20. Timoshenko, S. and Woinowsky-Krieger, S.: "Theory of Plates and Shells," Second Edition, Published by McGraw-Hill Book Company, Inc., N. Y., 1959.

21. Gawin, I.: "Tough Thermosetting Resins with Superior Damage Tolerance Hercules 8551 Series," Proceedings of the 31st International Sampe Symposium and Exhibition, April 1986, pp.1205-1213.

22. O'Brien, T. K., Murri, G. B. and Salpekar, S. A.: "Interlaminar Shear Fracture Toughness and Fatigue Thresholds for Composite Materials," Composite Materials: Fatigue and Fracture, Second Volume, ASTM STP 1012, P. A. Lagace, Ed., American Society for Testing and Materials, Philadelphia, 1989, pp.222-250.

23. Crews, J. H., Jr., Shivakumar, K. N., and Raju, I. S.: "Factors Influencing Elastic Stresses in Double Cantilever Beam Specimens," Adhesively Bonded Joints: Testing, Analysis, and Design, ASTM STP 981, W. S. Johnson, Ed., American Society for Testing and Materials, Philadelphia, 1988, pp.119-132.

24. Kanninen, M. F.: "A Dynamic Analysis of Unstable Crack Propagation and Arrest in the DCB Test Specimen," International Journal of Fracture, Vol. 10, No. 3, September, 1974, pp.415-430.

Table 1:- Comparison of DCB test results.

Material	$(G_{1c})_{initial}(J/m^2)$				$(G_{1c})_{average}(J/m^2)$	
Hinged	BM[a]	LB[b]	TB[c]	LDT[d]	Area	LDT[d]
T300/5208	94	107	-	107	112	119
IM7/8551-7	605	629	-	634	756	670
AS4/PEEK	1564	1593	-	1622	1705	1784
T- Tabbed						
T300/5208	96	102	107	107	85	100
IM7/8551-7	519	536	618	621	858	771
AS4/PEEK	1429	1401	1680	1734	1873	1805

[a] BM - Berry's method [17].

[b] LB - Present method neglecting tab and large deflection effects.

[c] TB - Present method considering only tab effects.

[d] LDT - Present method accounting for tab and large deflection effects.

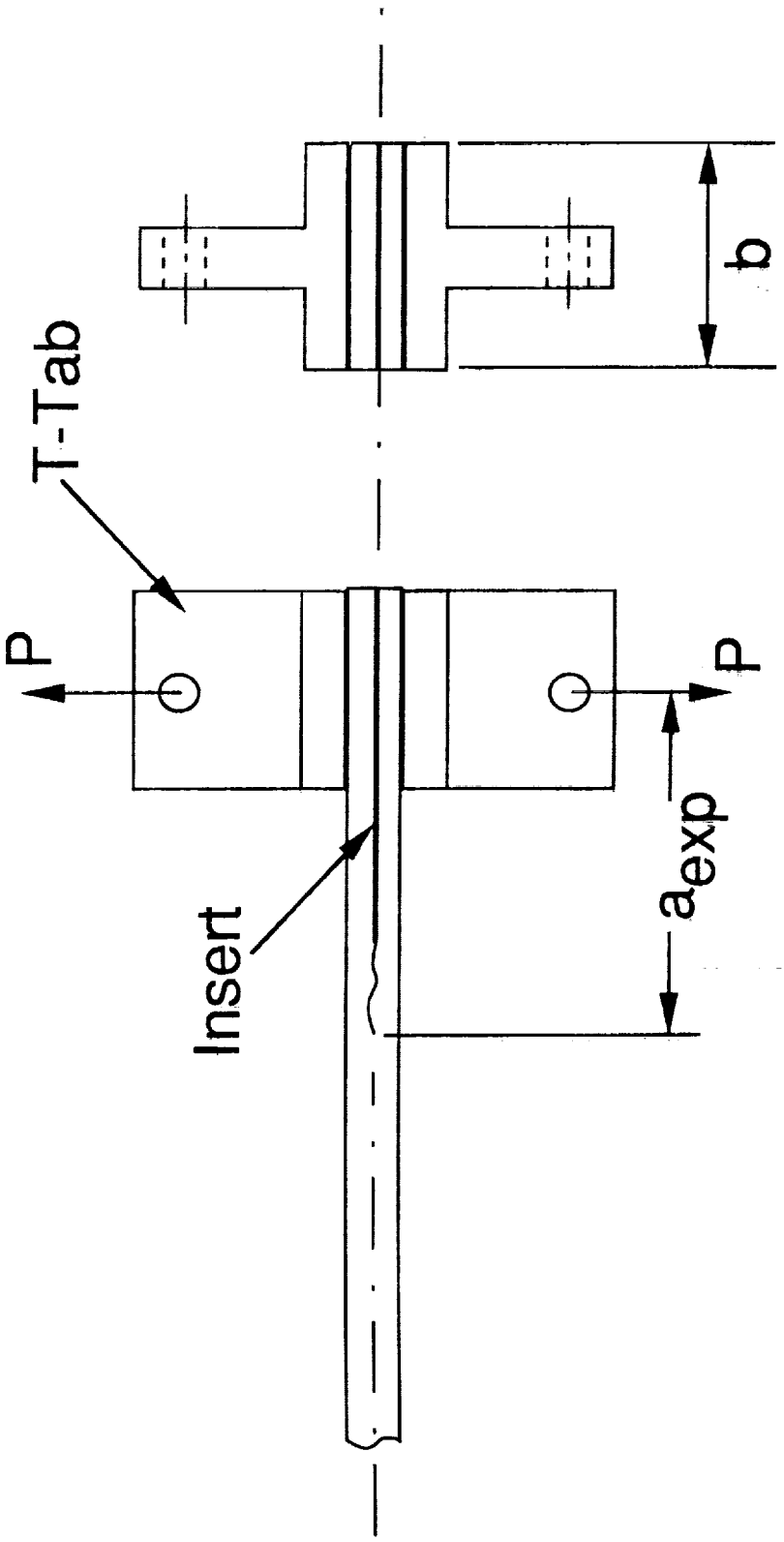

Figure 1.- DCB specimen with bonded T-tabs.

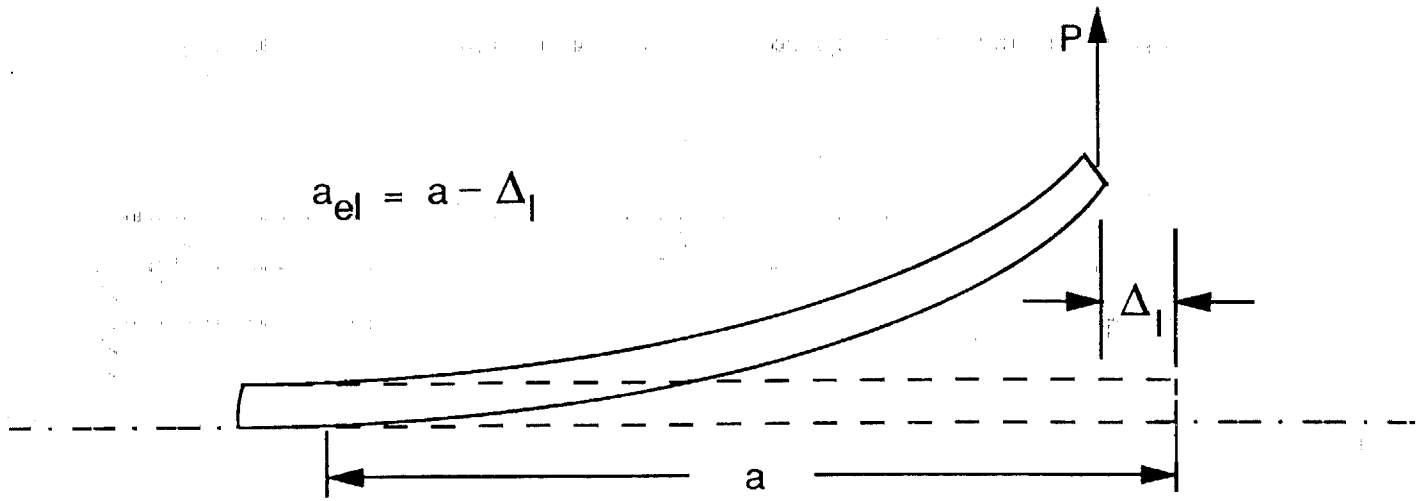

(a) Effect of large deflections

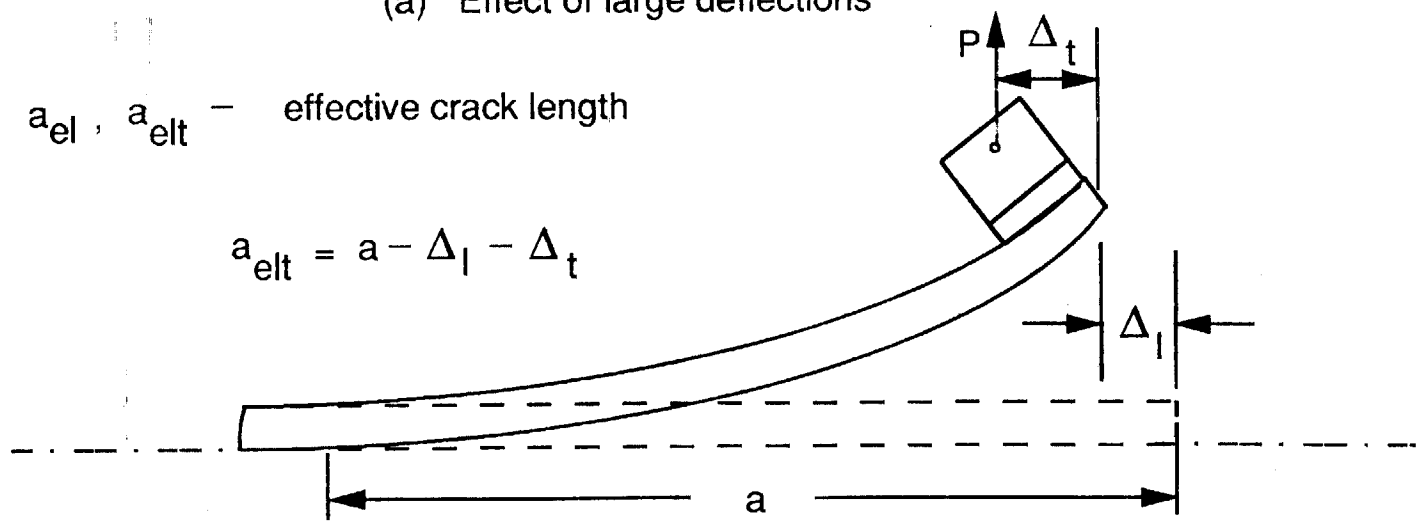

(b) Effect of large deflections and T-tabs

Figure 2.- Effects of large deflections and T-tabs in a DCB specimen test.

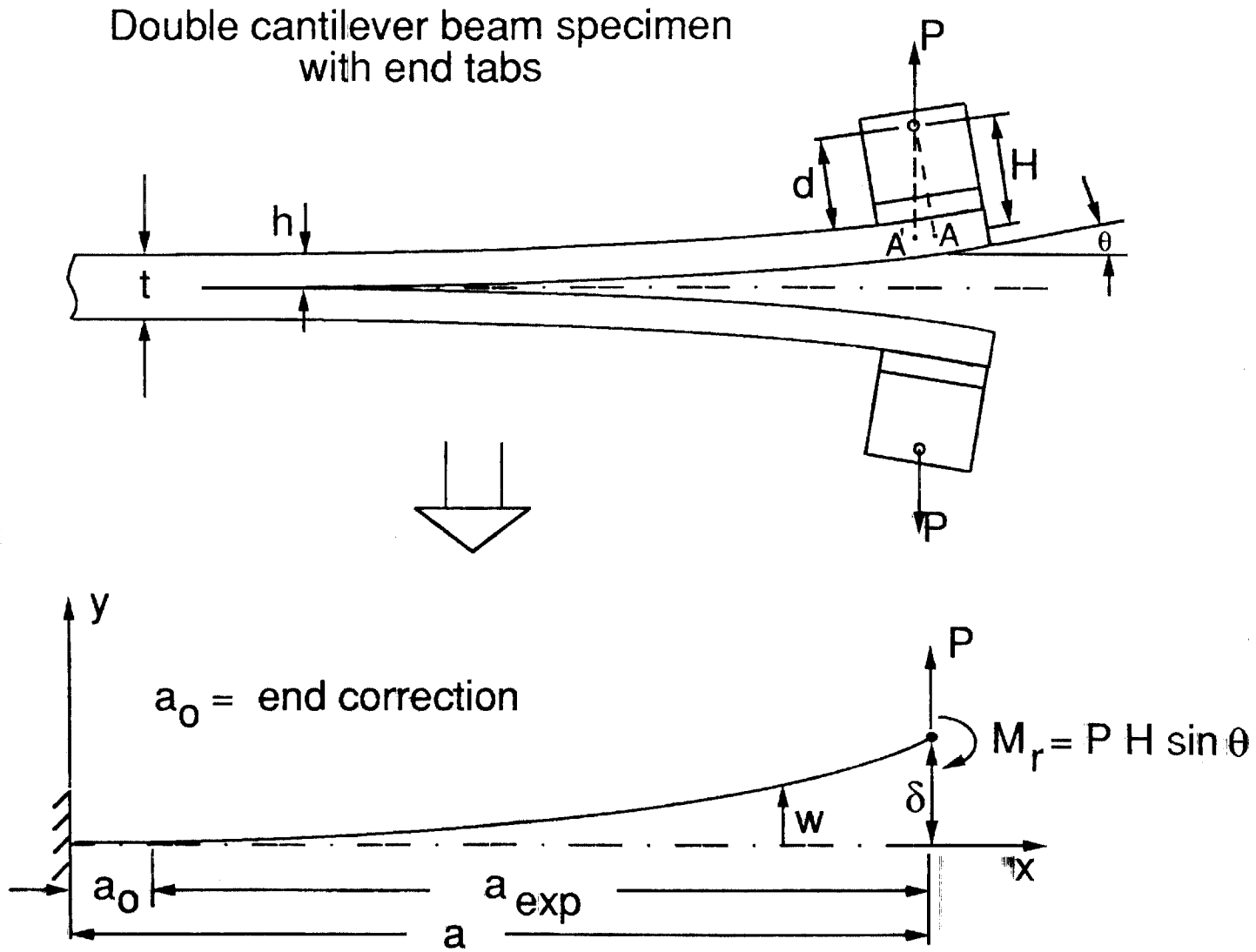

Figure 3.- Cantilever beam idealization for a DCB specimen with T-tabs.

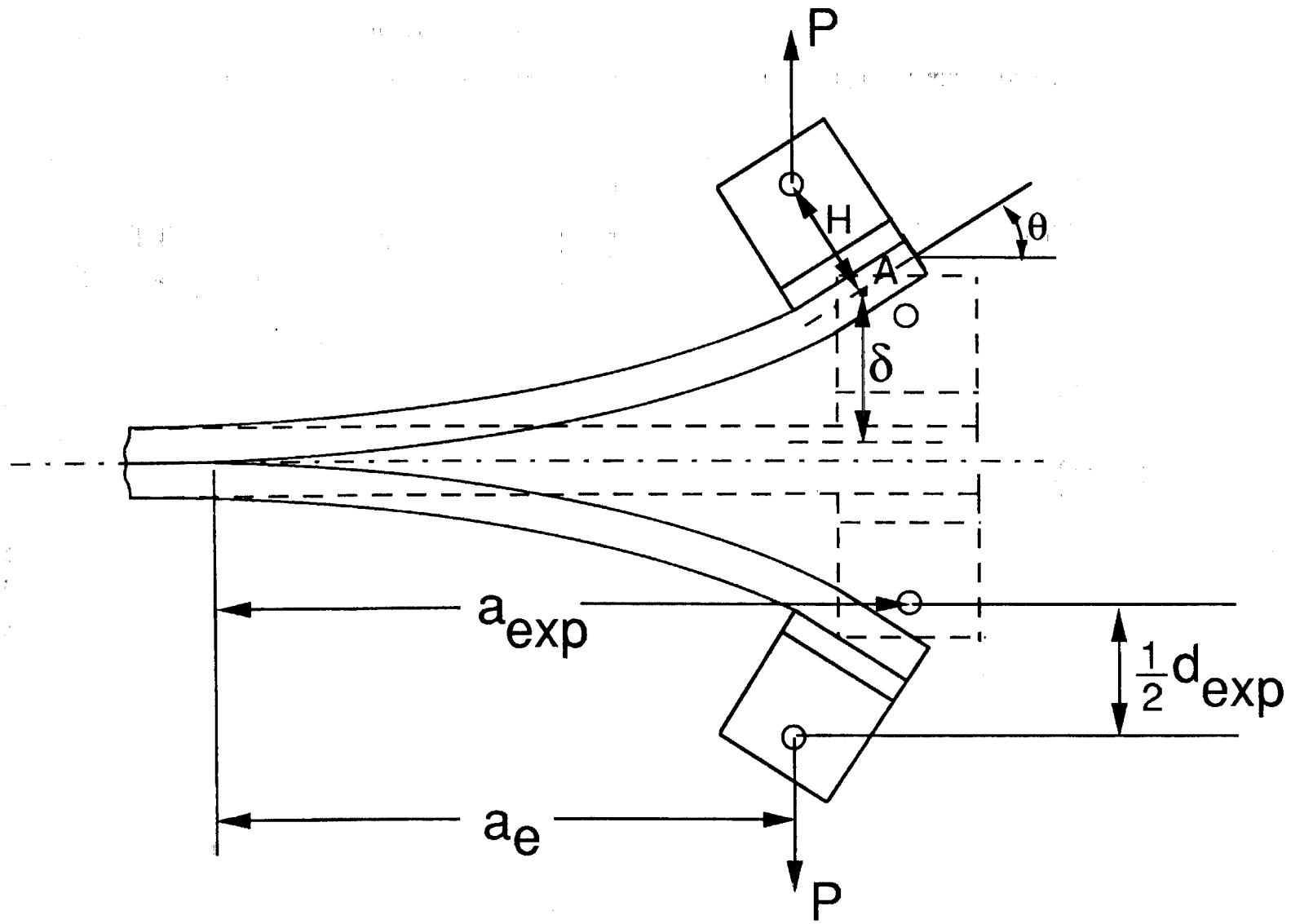

Figure 4.- Nomenclature for a DCB specimen with T-tabs.

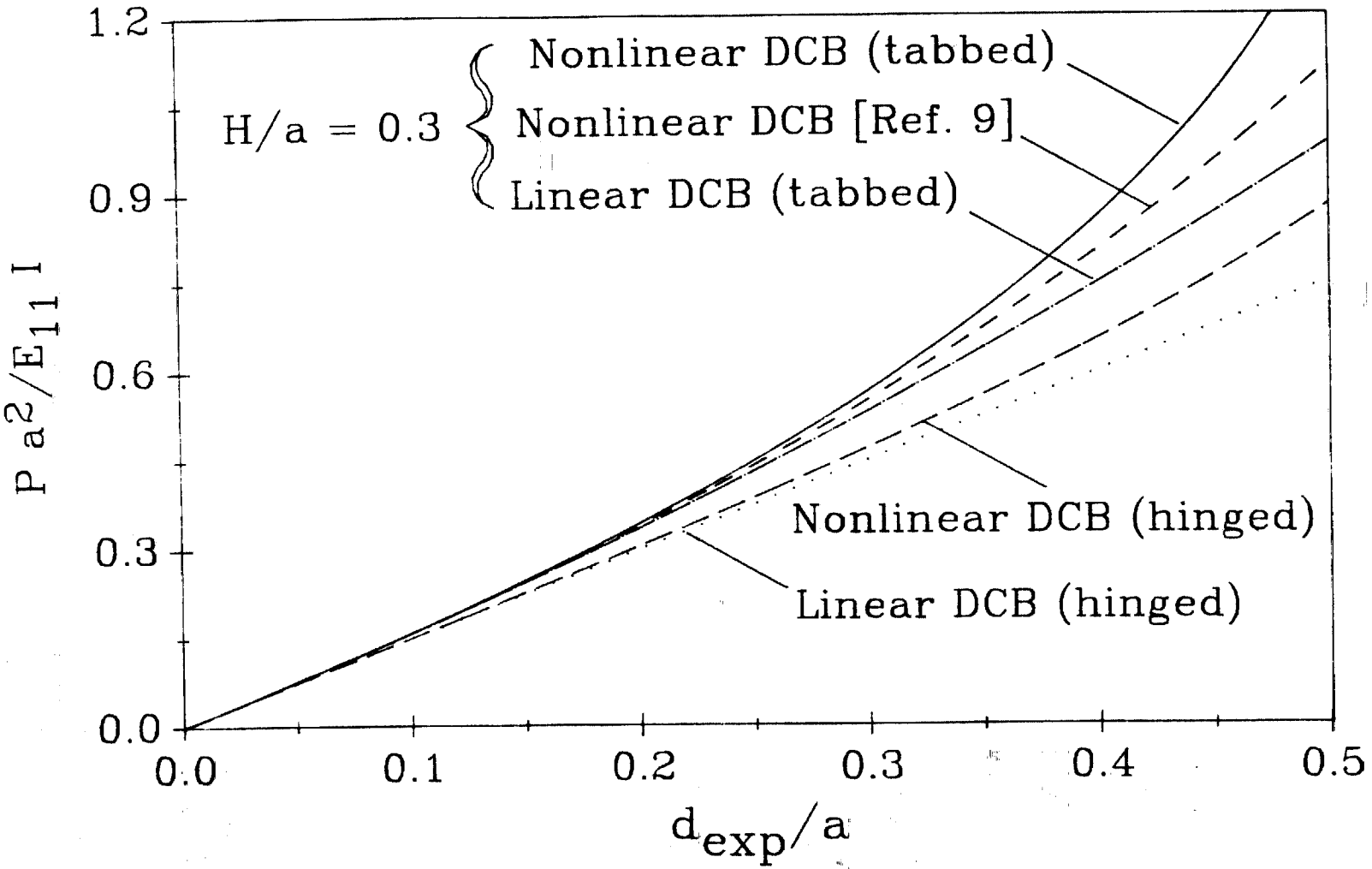

Figure 5.- Normalized load-deflection curves for hinged and tabbed DCB specimens.

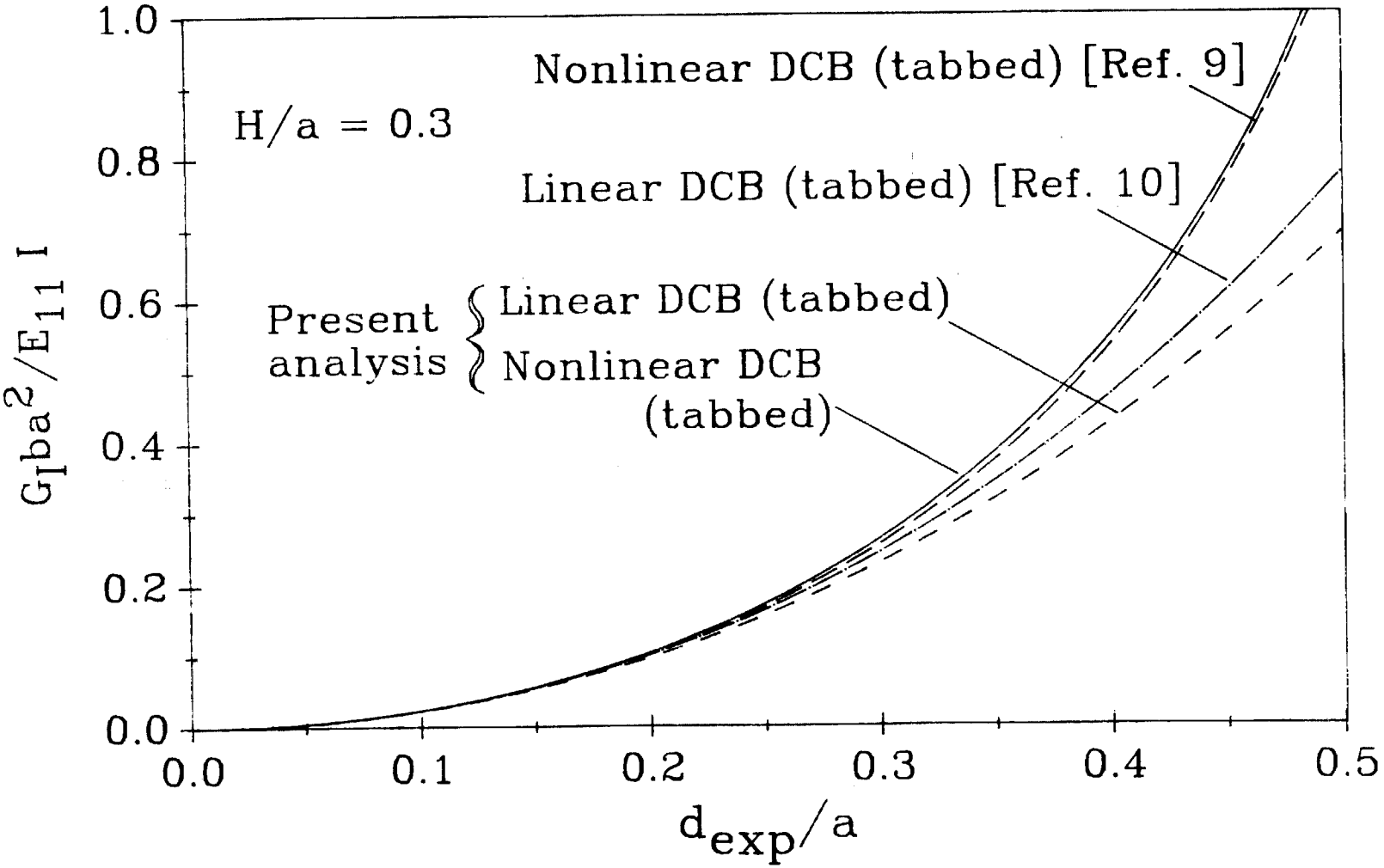

Figure 6.- Normalized strain-energy release rate curves for DCB specimens with T-tabs.

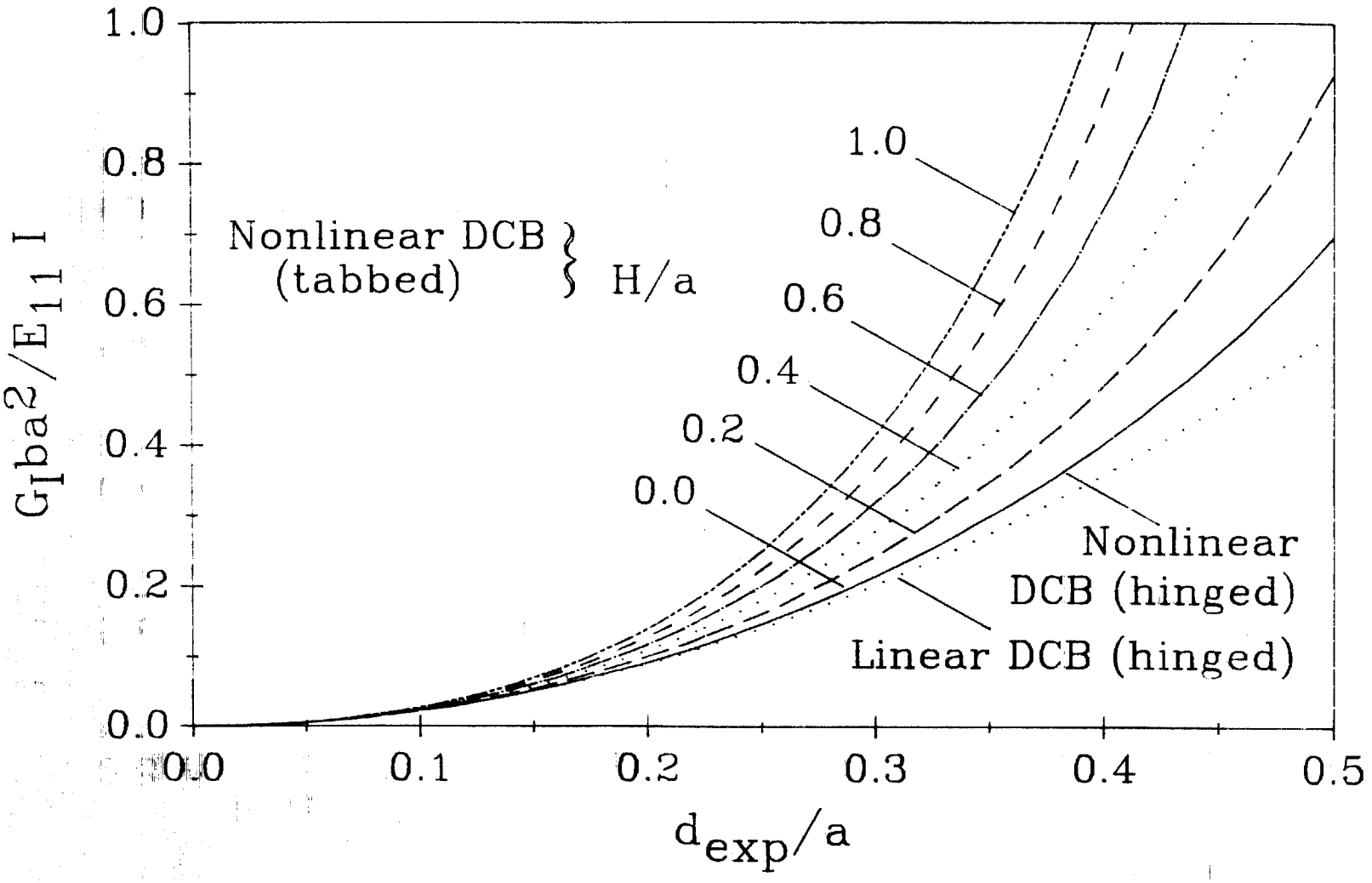

Figure 7.- Normalized strain-energy release rate curves for hinged and tabbed DCB specimens.

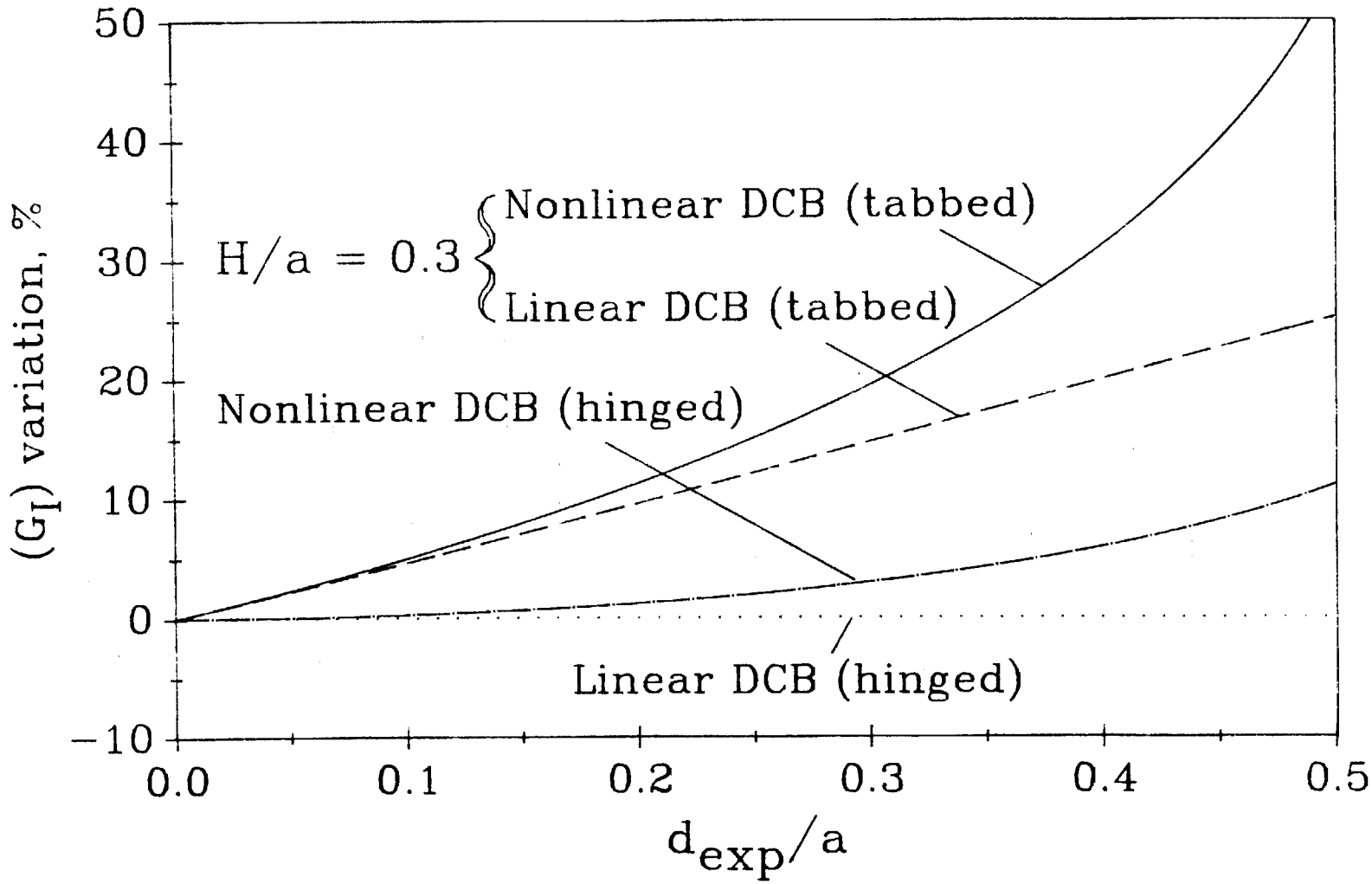

Figure 8.- Percentage variation in G_I for DCB specimens with geometric nonlinearities.

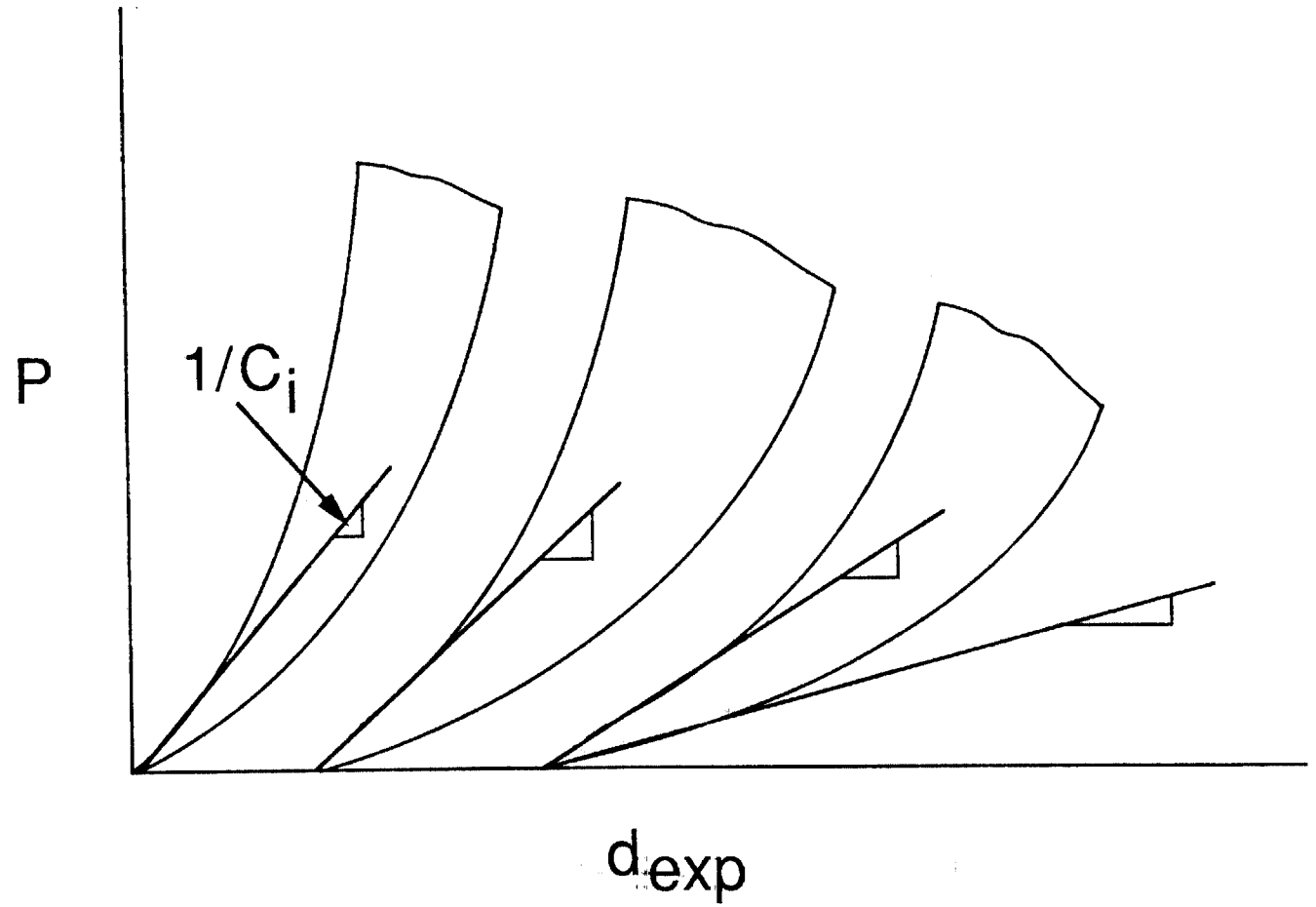

Figure 9.- Typical load-deflection curves for DCB specimens with geometric nonlinearities.

NASA National Aeronautics and Space Administration

Report Documentation Page

1. Report No.	2. Government Accession No.	3. Recipient's Catalog No.
NASA TM-101677		

4. Title and Subtitle

Effects of T-Tabs and Large Deflections in DCB Specimen Tests

5. Report Date

November 1989

6. Performing Organization Code

7. Author(s)

R. A. Naik and J. H. Crews, Jr., and K. N. Shivakumar

8. Performing Organization Report No.

10. Work Unit No.

505-63-01-05

9. Performing Organization Name and Address

NASA Langley Research Center
Hampton, VA 23665-5225

11. Contract or Grant No.

13. Type of Report and Period Covered

Technical Memorandum

12. Sponsoring Agency Name and Address

National Aeronautics and Space Administration
Washington, DC 20546

14. Sponsoring Agency Code

15. Supplementary Notes

R. A. Naik and K. N. Shivakumar, Analytical Services and Materials, Inc., Hampton, VA
J. H. Crews, Jr.: Langley Research Center, Hampton, VA

16. Abstract

A simple strength of materials analysis was developed for a double-cantilever beam (DCB) specimen to account for geometric nonlinearity effects due to large deflections and T-tabs. A new DCB data analysis procedure was developed to include the effects of these nonlinearities. The results of the analysis were evaluated by DCB tests performed for materials having a wide range of toughnesses. The materials used in the present study were T300/5208, IM7/8551-7, and AS4/PEEK.

Based on the present analysis, for a typical deflection/crack length ratio of 0.3 (for AS4/PEEK), T-tabs and large deflections cause a 15 percent and 3 percent effort, respectively, in the computed Mode I strain energy release rate. Design guidelines for DCB specimen thickness and T-tab height were also developed in order to keep errors due to these nonlinearities within 2 percent.

Based on the test results, for both hinged and tabbed specimens, the effects of large deflection on the Mode I fracture toughness (G_{Ic}) were almost negligible (less than 1 percent) in the case of T300/5208 and IM7/8551-7, however, AS4/PEEK showed a 2 to 3 percent effect. The effects of T-tabs on G_{Ic} were more significant for all the materials with T300/5208 showing a 5 percent error, IM7/8551 a 15 percent error, and AS4/PEEK a 20 percent error.

17. Key Words (Suggested by Author(s))	18. Distribution Statement
Double cantilever beam delamination fracture toughness composite large deflection	Unclassified - Unlimited Subject Category - 24

19. Security Classif. (of this report)	20. Security Classif. (of this page)	21. No. of pages	22. Price
Unclassified	Unclassified	41	A03